

## STABILITY AND DESIGN CRITERIA FOR UAV CONFIGURATIONS

Andrés Cremades Botella      ancrebo@etsid.upv.es

**Abstract**

In this article, aircraft configuration analysis is shown. The comparison between different geometries is developed for three operations. Transport operation, in this flight conditions the plane flights in straight line, with high speed and medium altitude approximately 500 m. Surveillance operation, the aircraft describes a circular flight with low altitude (100 m) and low velocity. Finally, humanitarian aid operation is evaluated, for this operation, low altitude, high velocity and small radius of turn is required. Along the article advantages and disadvantages for the different operations of each configuration are shown. In addition, an analysis of eigenvalues is conducted, evaluating also a variation on the center of gravity position and its effects in stability.

**Nomenclature**

$\alpha$	Angle of attack	$L$	Lift
$\gamma$	Flight slope	$m$	Mass
$\Delta E_c$	Kinetic energy variation	$n$	Load factor
$\delta_p$	Percentage of battery voltage	$P$	Engine power
$\eta_p$	Propeller efficiency	$P_2$	Climbing power
$\theta$	Propeller geometry angle	$P_{TO}$	Take off power
$\lambda_i$	Adimensional induced velocity	$Q$	Propeller moment
$\lambda_z$	Adimensional axial velocity	$R$	Propeller radius
$\mu$	Friction coefficient	$R_{TO}$	Take off distance
$\rho$	Density	$R_L$	Landing distance
$\phi$	Induced angle	$S_w$	Wing surface
$\Omega$	Propeller angular velocity	$T$	Thrust
$AE$	Aerodynamic efficiency	$v$	Velocity
$b$	Number of blades	$V_3$	Landing velocity
$C_D$	Drag coefficient	$V_b$	Battery voltage
$C_L$	Lift coefficient	$V_i$	Induced velocity
$C_Q$	Moment coefficient	$V_{LO}$	Lift off velocity
$C_T$	Thrust coefficient	$V_z$	Axial velocity
$D$	Drag	$V_{stall}$	Stall velocity
$F_{roz}$	Friction force on the wheels	$W_e$	Empty weight
$F_T$	Propeller resistance force	$x$	Propeller radial adimensional position
$g$	Gravity acceleration		
$K_v$	Engine angular velocity coefficient		

# Introduction

Unmanned aerial vehicles (UAVs) are a hot topic in the Aerospace Industry and are currently experiencing important developments. Their versatility has a great number of advantages in some flight operations as transport, surveillance and military missions. UAVs industry is creating a high number of high-skilled jobs, while positively contributing to the general economy. As they can be manufactured in sizes, weights and shapes much different than the typical manned vehicle, some of the tendencies used to design other aircraft might not be applicable. Therefore, it is important to establish criteria for their design in order to increase their efficiency and improve their performance.

In the following article, the design and stability criteria for different configurations of electric and low cost UAVs is shown, for a maximum take-off weight of around 7 kg. The influence of geometric parameters is analysed in different operations: transport, surveillance and humanitarian aid. Aerodynamic and propulsive parameters are analysed for the different configurations and flight operations. Finally, a comparison of the configuration and their advantages is shown. In order to establish the previous criteria, a computer tool of fast calculation will be developed.

For the mathematical model of the aeroplane, USAF DATCOM [1] will be scanned and applied. Furthermore, xflr5 [5] is used in order to compare aerodynamic efficiency and pathlines of each configuration. In addition, for the thrust model, blade element theory is utilised. These theories are applied to the computer tool. The article also includes weight analysis of the aircraft. To estimate their structural weight similar aeroplanes will be used. Aircraft data is obtained from UPC Venturi [3] and UPC Trencalòs [4] (both teams from Air Cargo Challenge competition held in Zagreb in 2017). With these aeroplanes a relation between maximum take-

off weight and operating empty weight will be obtained. Regressions will give an estimated value of operating empty weight. In addition, a more accurate calculus of the weight will be done. For this calculus, carbon fibre mono-coque structure of 0.55 mm of thickness will be considered, two engines of 350 g and electronic equipment of 600 g. Electronic equipment includes weight of batteries and autopilot. Maximum take off weight of every aircraft is the same 6.9 kg. Payload weight is the difference between maximum take-off weight (MTOW) and operating empty weight.

## Studied configurations

Along the article three different configurations will be studied. Aircraft configurations are compared in order to determine the most appropriated one for each operation. As said before, empty weight is compared with Air Cargo Challenge planes. The regression curve obtained from the competition planes is:

$$W_e = 1.217 + 2.9978S_w \quad (1)$$

- Configuration 1: double tail configuration, as shown in Figure 1. This configuration is studied because it is a known geometry. Many planes shows it. It is also a compact configurations and it is supposed to be an stable geometry.

This configuration has an empty weight of 4.2 kg assuming carbon fibre structure. And approximately 4.1 kg assuming previous regression.

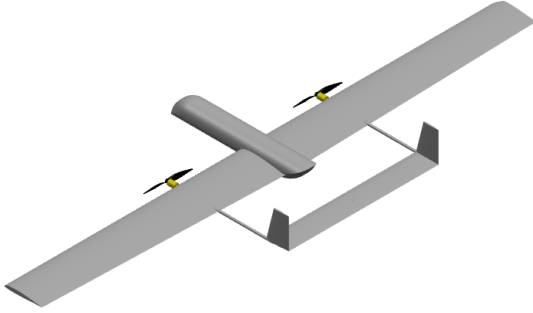


Figure 1: Configuration 1 sketch.

- Configuration 2: Canard configuration with stabilisers in wing tips, as shown in Figure 2. With this configuration it is expected to obtain the most efficient aircraft because of the contribution of canard in the generation of lift. Canard also offers some protection against stall. Nevertheless, the longitudinal stability of canard aeroplanes is much more difficult than conventional configuration. For this reason, it will require a more complex control systems to drop payload in humanitarian aid missions.

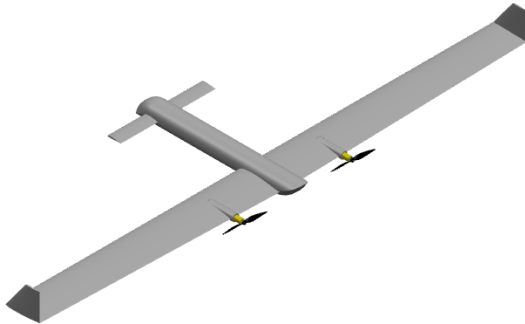


Figure 2: Configuration 2 sketch.

This geometry has 4.3 kg of empty weight assuming a carbon fibre monocoque. However, it weights 4.2 kg if regression is used.

- Configuration 3: Three surface configuration with double tail, as shown in Figure 3. The objective of this configuration

is to obtain canard configuration advantages while avoiding its stability problems. This geometry has extra capacity to move its centre of gravity without turning it to an unstable configuration.

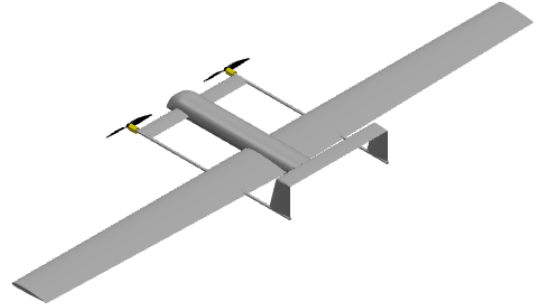


Figure 3: Configuration 3 sketch.

Assuming a carbon fibre monocoque structure, this geometry has an empty weight of 4.3 kg. This structural weight is higher than previous configurations due to the number of lifting surfaces. Nevertheless, applying regression a weight of 4.2 kg is obtained.

In the following calculation carbon fiber weight is assumed in order to know exact position of the center of gravity.

## Operation diagram

In order to establish wing dimensions and choose engines it is important to represent the operation diagram. In this figure it is shown power weight ratio versus wing load. The operation diagram represents the different operations of flight: cruise, take-off, climb, landing and turns.

- Cruise: force equilibrium is imposed:

$$L = mg \quad (2)$$

$$T = D \quad (3)$$

Equation 3 is divided by equation 2.

$$\frac{T}{m} = g \frac{D}{L} \quad (4)$$

Assuming that  $T = \frac{P\eta_p}{v}$ :

$$\frac{P_{TO}}{m} = \frac{vg}{\eta_p} \frac{1}{AE} \frac{P_{TO}}{P} \quad (5)$$

Observing Equation 16 it can be shown that to reduce the power needed in cruise flight it is important to increase both the aerodynamic and propulsive efficiencies. Equation 16 is a simplified expression from a blade element thrust model. In the following computations, calculated power is obtained from blade element theory.

- Take-off: to calculate this operation is needed to make an energy balance:

$$\Delta E_c = (T - D - F_{roz})R_{TO} \quad (6)$$

where  $F_{roz} = \mu(mg - L)$  and velocity is set as a medium value between zero and lift off velocity  $V_{LO} = 1.2V_{stall}$  and thrust is obtained from blade element method.

$$\frac{P_{TO}}{m} = \frac{v_{TO}}{\eta_p} \left( \frac{v_{LO}^2}{2R_{TO}} - \frac{\mu L}{m} + \frac{D}{m} + \mu g \right) \quad (7)$$

- Climb: force equilibrium is imposed.

$$T = D + W\gamma \quad (8)$$

$$L = W \quad (9)$$

Dividing Equation 8 by Equation 9:

$$\frac{T}{mg} = \frac{D}{L} + \gamma \quad (10)$$

And assuming simplified expression for thrust:

$$\frac{P_{TO}}{m} = \frac{gv}{\eta_p} \left( \frac{1}{AE} + \gamma \right) \frac{P_{TO}}{P_2} \quad (11)$$

To reduce the power needs in a constant slope climb is important to increase the aerodynamic and propulsive efficiencies.

- Landing: is calculated with an energy balance.

$$\Delta E_c = (-D - F_{roz})R_L \quad (12)$$

obtaining the following expression for the curve:

$$\frac{m}{S_w} = \frac{\rho v_1^2 (C_L \cdot \mu - C_D)}{2\mu g - \frac{v_3^2}{R_L}} \quad (13)$$

- Turns: the force equilibrium is solved:

$$L = mgn \quad (14)$$

$$T = D \quad (15)$$

Dividing Equation 15 by Equation 14, the curve equation is obtained.

$$\frac{P_{TO}}{m} = \frac{vng}{\eta_p} \frac{1}{AE} \frac{P_{TO}}{P} \quad (16)$$

Wing load is optimised in order to be as high as possible. For the different configurations the following diagrams are obtained.

- Geometry 1:

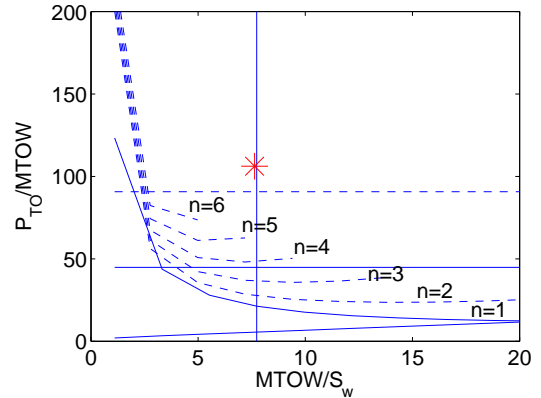


Figure 4: Operation diagram of geometry 1.

- Geometry 2:

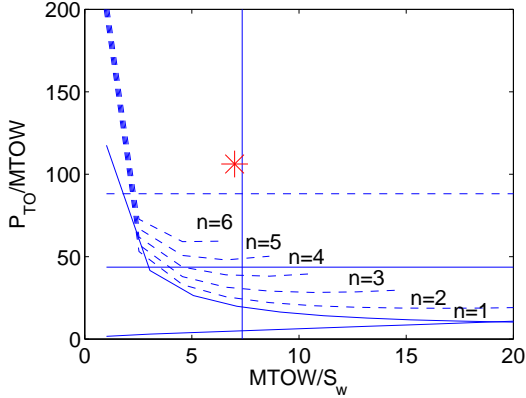


Figure 5: Operation diagram of geometry 2.

- Geometry 3:

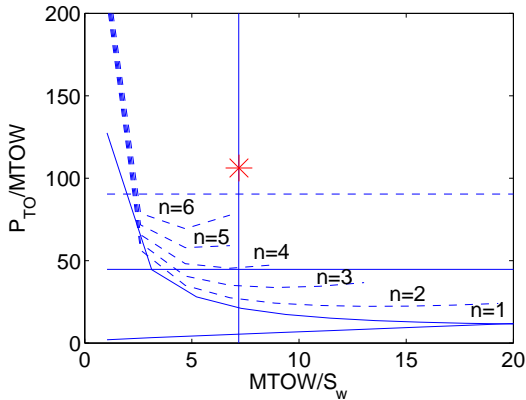


Figure 6: Operation diagram of geometry 3.

## Theoretical background

In the article, USAF DATCOM [1] is utilized to obtain the aerodynamic coefficients. DATCOM take use of semi-empirical procedures to calculate aerodynamics. With these coefficients it is possible to obtain aerodynamic moments and forces, which are utilized in equations of mechanics applied to a body with six degrees of freedom: force equations (33, 34 and 35), moment equations (39, 40 and 41), Euler equations (46, 47 and 48) and finally kinematic equations (49, 50 and 51).

Linearizing the previous equations it is possible to obtain movement eigenvalues of the aircraft. The eigenvalues are associated with the different modes of movement:

- Short period: it is a longitudinal oscillatory mode with high damping and frequency.
- Phugoid: it is a longitudinal oscillatory mode with low damping and frequency.
- Dutch roll: it is a lateral-directional oscillatory mode.
- Roll subsidence mode: it is a lateral-directional non-oscillatory mode with high damping.
- Spiralling: it is a lateral-directional non-oscillatory mode with low damping.

The previous flight modes determine the stability of the aeroplane and they must be studied in order to design an aircraft which does not need complex autopilot systems.

On the other hand, to model the propulsive system, blade element theory has been utilized. In this theory aerodynamics of each section of the blade are calculated. Then 3D corrections are added to the model to correct tip effects. A sketch of the section is shown in Figure 7.

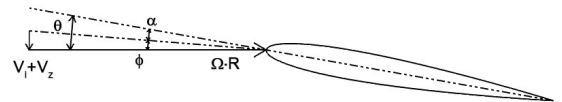


Figure 7: Blade element sketch.

As shown in Figure 7:

$$\theta = \alpha + \phi \quad (17)$$

where  $\phi$  represents the induced angle of the velocity, which is produced by the rotation of the propeller.

$$\phi = \arctan\left(\frac{V_i + V_z}{\Omega R}\right) \quad (18)$$

Nondimensionalising the parameters the following expression is obtained:

$$\phi = \arctan(\lambda_i + \lambda_z) \quad (19)$$

where,

$$\lambda_i = \frac{V_i}{\Omega R} \quad (20)$$

$$\lambda_z = \frac{V_z}{\Omega R} \quad (21)$$

Thrust is generated by lift and drag coefficients of the blade according to the following equation:

$$T = L \cos\phi - D \sin\phi \quad (22)$$

The rotation resistance of the blade is also calculated. This force is used to obtain the power needed to move the propeller:

$$F_T = L \sin\phi + D \cos\phi \quad (23)$$

and torque:

$$Q = r (L \sin\phi + D \cos\phi) \quad (24)$$

Nondimensionalising thrust and torque:

$$c_T = \frac{T}{\rho \pi R^4 \Omega^2} \quad (25)$$

and

$$c_Q = \frac{Q}{\rho \pi R^5 \Omega^2} \quad (26)$$

Torque coefficient is equal than power coefficient. For this reason is possible to know the power required by the rotation. To solve blade element method it is needed to know the induced velocity in each section of the blade. Blade element thrust must be equal to the conservation of linear momentum. Induced velocity is modified to include 3D effects:

$$\lambda_i = \frac{dc_T}{4x F (\lambda_i + \lambda_z)} \quad (27)$$

being,

$$F = \frac{2}{\pi} a \cos(e^{-f}) \quad (28)$$

$$f = \frac{b}{2} \frac{1-x}{x\phi} \quad (29)$$

This way it is possible to obtain a expression of thrust and power as a function of nondimensional velocity. In order to calculate the nondimensional velocity is needed to know the rotational velocity of the blade. This velocity is obtained directly from the specifications of the engine. Rotational velocity is proportional to the applied voltage. Rotational speed is obtained in equation 30.

$$\Omega = K_v V_b \delta_p \quad (30)$$

being  $\delta_p$  the control of the battery voltage and the control of aircraft thrust. Voltage needed to maintain required thrust and power applied on the propeller gives a value of current intensity. The intensity utilised to give power to the engine determines the battery consumption. The aircraft analysed in this article is able to give 2200 mA h. This fact means that the battery can maintain a current of 2.2 A during 1 h. The autonomy of the aircraft in flying condition is determined making use of previous parameters. Range is calculated from previous calculus multiplying autonomy by flight velocity.

## Operations comparison

In this section studied operation comparison is shown. The first item to compare is flight domain. It is important to know the conditions in which every configuration can flight. Flight domain is calculated establishing force equilibrium in both axis (two-dimensional problem).

$$L = W \quad (31)$$

$$D = T \quad (32)$$

Comparing previous configurations the following diagram is obtained.

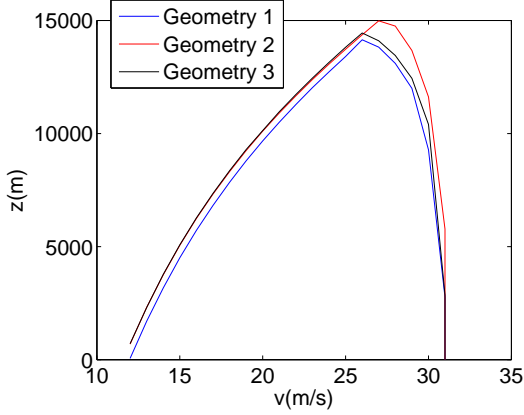


Figure 8: Flight domain comparison.

It can be shown that canard configuration is able to have slightly higher flight conditions. This fact is an important advantage for military aeroplanes and can be decisive in combat maneuvers. Moreover, for civil configurations there is not an important difference between studied configurations. This fact is due to higher aerodynamic efficiency of geometry 2. In Figure 9 a comparison (without fuselage influence) between studied configuration is presented.

Figure 9 shows that canard configuration presents higher aerodynamic efficiency. For this reason, in Figure 8 geometry 2 has the highest flight domain. Canard configuration has higher aerodynamic efficiency because of the reduction of induced drag generated by the lifting elevator (canard). Studied configurations are shown in Figure 21.

Operations must be determined in order to study plane behaviour in these conditions. In this section are evaluated three flight conditions: transport (velocity  $30 \text{ m s}^{-1}$ , altitude  $500 \text{ m}$ ), surveillance mission (velocity  $15 \text{ m s}^{-1}$ , altitude  $100 \text{ m}$ , radius  $500 \text{ m}$ ) and

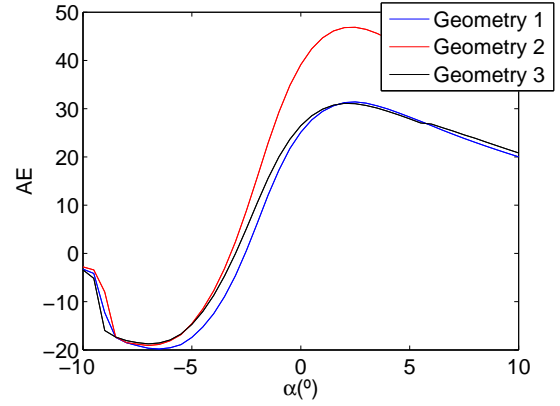


Figure 9: Comparison of aerodynamic efficiency for different wing configuration. Values obtained with xflr5 [5].

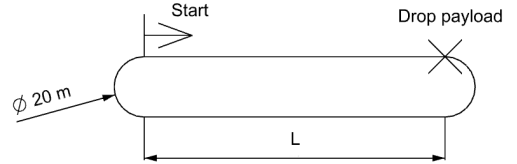


Figure 10: Human aid trajectory.

humanitarian aid (velocity  $20 \text{ m s}^{-1}$ , altitude  $100 \text{ m}$ , radius of the curves of  $10 \text{ m}$  dropping  $500 \text{ g}$  of payload before the first curve), in this mission the aircraft draws the trajectory shown in Figure 10.

Another objective of the article is to reduce the complexity of autopilot systems for this reason is important to design a stable aircraft. To evaluate stability of the aeroplane both longitudinal and lateral-directional eigenvalues are analysed. This eigenvalues are evaluated for every point of the flight domain. Results are plotted in the appendix of the article. In the following table, eigenvalues are evaluated for flight operations.

<b>Transport</b>		
Geometry 1	Geometry 2	Geometry 3
-10.20+18.00i	-12.72+16.82i	-13.68+21.03i
-10.20-18.00i	-12.72-16.82i	-13.68-21.03i
-0.18+0.38i	-0.18+0.34i	-0.19+0.36i
-0.18-0.38i	-0.18-0.34i	-0.19-0.36i
-17.06	-13.54	-16.09
-0.38+3.25i	-1.58	-0.26+2.18i
-0.38-3.25i	1.12	-0.26-2.18i
0.02	0.03	0.004

Table 1: Eigenvalues for transport flight.

It can be seen that geometry 1 and 3 present a similar behaviour. For geometry 3, longitudinal modes are more damped because the higher number of horizontal stabilizers. Three configurations are lateral-directional unstable. Nevertheless, geometry 1 and 3 only presents an unstable mode (spiralling) which is slow and can be corrected by a human pilot or a simple automatic control system. Spiralling mode means that plane is unable to correct its rolling motion and it is aligned with relative wind loosing altitude and drawing a spiral motion.

On the other hand, geometry 2 presents two unstable modes and it needs an autopilot to be controlled.

Eigenvalues are also evaluated in surveillance operations:

<b>Surveillance</b>		
Geometry 1	Geometry 2	Geometry 3
-5.32+9.18i	-6.64+8.63i	-7.14+10.81i
-5.32-9.18i	-6.64-8.63i	-7.14-10.81i
-0.09+0.83i	-0.09+0.74i	-0.10+0.79i
-0.09-0.83i	-0.09-0.74i	-0.10-0.79i
-9.25	-7.34	-8.79
-0.55+1.52i	-1.13	-0.37+0.95i
-0.55-1.52i	0.33+0.29i	-0.37-0.95i
0.12	0.33-0.29i	0.04

Table 2: Eigenvalues for surveillance flight.

As happened before, both geometries 1 and 3 show similar modes. These configurations present an unstable lateral-directional mode, spiralling. Moreover, geometry 2 presents unstable dutch roll. This instability happens because lateral stability is much higher than directional, which means that aircraft will restore rolling motion faster than it corrects its side-slip so it passes flight level.

Finally, eigenvalues for humanitarian aid are evaluated. To know the behaviour of the aeroplane in this operation it is needed to analyse both straight flight and curves.

On the first hand, straight flight eigenvalues are evaluated:

<b>humanitarian aid: straight flight</b>		
Geometry 1	Geometry 2	Geometry 3
-7.07+12.20i	-8.81+11.41i	-9.46+14.24i
-7.07-12.20i	-8.81-11.41i	-9.46-14.24i
-0.13+0.62i	-0.12+0.55i	-0.13+0.59i
-0.13-0.62i	-0.12-0.55i	-0.13-0.59i
-11.95	-9.47	-11.24
-0.40+2.17i	-1.18	-0.27+1.45i
-0.40-2.17i	0.66	-0.27-1.45i
0.07	0.13	0.05

Table 3: Eigenvalues for humanitarian aid flight.

Aeroplane configurations behaviour is the same than the one obtained in transport operations. It show weak lateral-directional stability in geometry 2.

On the other hand, eigenvalues from curves of 10 m of radius are analysed. This curves have a small radius, because the plane must drop the payload and come back as fast as possible. Eigenvalues are shown in Table 4.

In Table 4 it can be seen that geometry 1 is the most stable in closed curves. Moreover, geometry 2 and 3 present instability in dutch roll mode.

<b>humanitarian aid: curves</b>		
Geometry 1	Geometry 2	Geometry 3
-3.67+13.32i	-5.49+11.54i	-6.16+14.82i
-3.67-13.32i	-5.49-11.54i	-6.16-14.82i
-0.05+0.66i	-0.04+0.64i	-0.05+0.65i
-0.05-0.66i	-0.04-0.64i	-0.05-0.65i
-14.94	-11.20	-14.49
-0.15+0.64i	-2.69	-3.09
-0.15-0.64i	0.57+0.53i	0.24+0.74i
-3.25	0.57-0.53i	0.24-0.74i

Table 4: Eigenvalues for humanitarian aid flight.

Another important fact of the comparison of previous geometries is the influence of the variation of the centre of gravity in the stability of the aircraft. The analysis will check the value of the eigenvalues if the centre of gravity moves 30% of the wing chord forward and backward. This analysis is made for  $20 \text{ m s}^{-1}$  and 100 m of altitude.

In Tables 5 and 6 it is shown that geometry 3 is the most stable against changes on the centre of gravity of the aeroplane. This fact makes this configuration the most appropriated for dropping humanitarian aid. In Table 5 is shown that geometry 3 stays stable with the variation of the center of gravity, on the contrary, geometry 1 and 2 become unstable. On the other hand, in Table 6 every geometry is stable. When the center of gravity moves forward, airplane becomes more stable and it is necessary to know the deflection of the longitudinal stabilizer. For geometry 1 elevator deflection is increased in  $1.71^\circ$ . In geometry 2 is needed to deflect  $2.03^\circ$  more than original center of gravity position. Finally, for geometry 3 canard stays in the same position and elevator is deflected  $3.71^\circ$  from original position. It is important to observe that geometry 3 has two degrees of freedom. Canard can be deflected to correct elevator's deflexion.

<b>Centre of gravity movement: backward.</b>		
Geometry 1	Geometry 2	Geometry 3
-17.91	-13.68	-9.23+4.16i
4.23	-3.93	-9.23-4.16i
-0.18+0.80i	-0.66	-0.14+0.30i
-0.18-0.80i	0.27	-0.14-0.30i
-11.94	-9.48	-11.22
-0.39+2.18i	-1.20	-0.26+1.46i
-0.39-2.18i	0.65	-0.26-1.46i
0.07	0.14	0.05

Table 5: Eigenvalues for movement of the centre of gravity: 30 % backward.

<b>Centre of gravity movement: forward.</b>		
Geometry 1	Geometry 2	Geometry 3
-8.35+20.03i	-9.47+16.44i	-10.58+19.24i
-8.35-20.03i	-9.47-16.44i	-10.58-19.24i
-0.13+0.65i	-0.13+0.62i	-0.13+0.63i
-0.13-0.65i	-0.13-0.62i	-0.13-0.63i
-11.97	-9.45	-11.26
-0.42+2.16i	-1.17	-0.29+1.44i
-0.42-2.16i	0.67	-0.29-1.44i
0.08	0.12	0.06

Table 6: Eigenvalues for movement of the centre of gravity: 30 % forward.

Assuming that maximum deflection for both canard and elevator is  $10^\circ$ , maximum forward center of gravity movement is shown in Figure 7. And maximum variation of the center of gravity is presented on the Table 8.

<b>Centre of gravity: limit position.</b>		
Geometry 1	Geometry 2	Geometry 3
$-1.36 c_w$	$-0.9 c_w$	$-1.42 c_w$

Table 7: Maximum forward center of gravity position.

Maximum variation of the center of gravity		
Geometry 1	Geometry 2	Geometry 3
$1.76 c_w$	$2.48 c_w$	$6.21 c_w$

Table 8: Maximum variation of the center of gravity.

In Table 8 it is shown that geometry 3 presents higher variation of the center of gravity. In this geometry the position of the center of gravity can change much more than in geometry 1 and 2. For this reason, airplane 3 has greater advantages for dropping loads than aircrafts 1 and 2.

Moreover, the higher number of degrees of freedom of the geometry 3 permit to increase aerodynamic efficiency of the airplane for a defined flight conditions.

In addition, it is analysed the influence of wing load and propeller diameter to obtain the better performance in operations. For geometry 1 the following results are obtained:

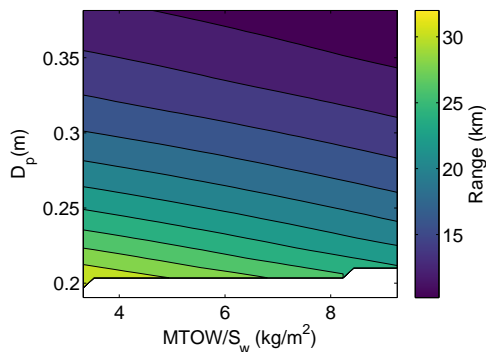


Figure 11: Geometry 1: Transport performance.

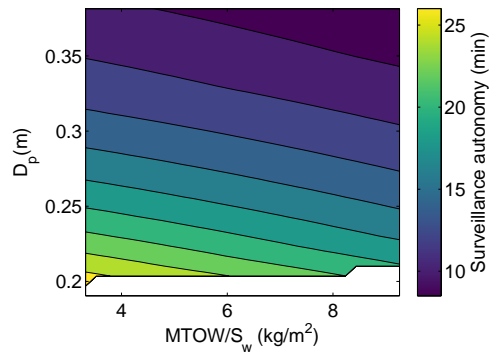


Figure 12: Geometry 1: Surveillance performance.

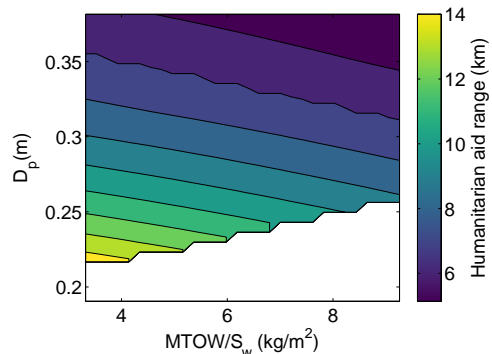


Figure 13: Geometry 1: humanitarian aid performance.

It is shown that to increase the range and endurance of the aeroplane it is needed to decrease the propeller diameter inside some limits of thrust. For the other configurations results are similar:

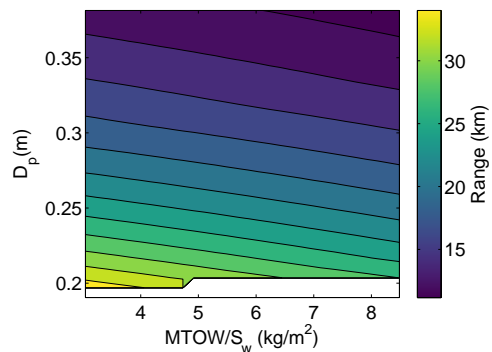


Figure 14: Geometry 2: Transport performance.

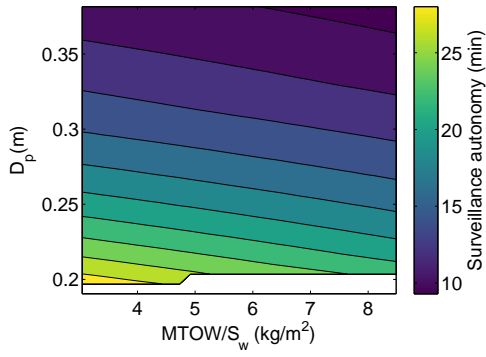


Figure 15: Geometry 2: Surveillance performance.

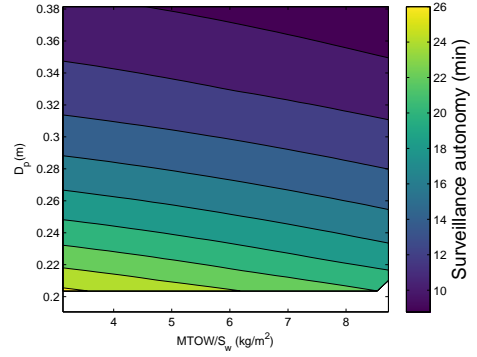


Figure 18: Geometry 3: Surveillance performance.

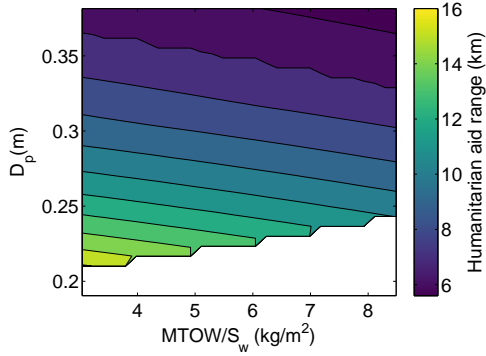


Figure 16: Geometry 2: humanitarian aid performance.

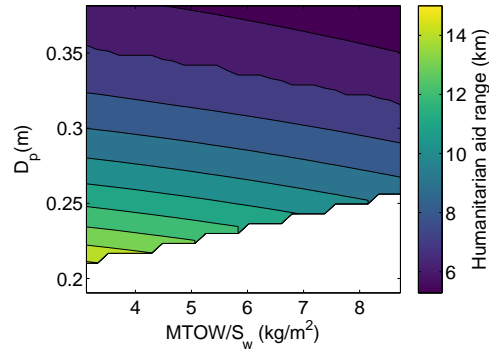


Figure 19: Geometry 3: humanitarian aid performance.

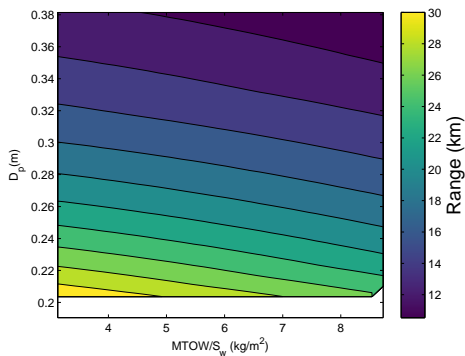


Figure 17: Geometry 3: Transport performance.

It can be seen that geometry 2 presents better performance than geometry 1 and 3. This fact is due to canard configuration. Canard is a lifting surface which helps in the generation of lift, reducing main wing lift and induced drag. For this reason geometry 2 works better in transport and surveillance missions. Nevertheless in humanitarian aid mission the selection of the configuration depends on the wingload and propeller diameter, as shown in Figure 20.

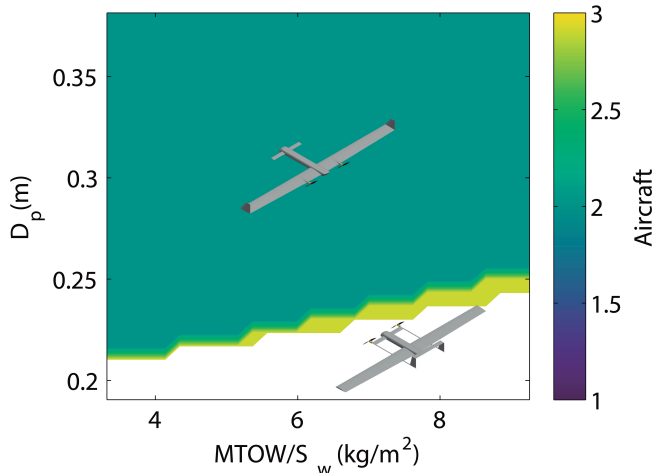


Figure 20: humanitarian aid: geometry selection.

It can be shown that for maximum distance of humanitarian aid geometry 2 must be used. This fact is the result of its higher aerodynamic efficiency. Nevertheless, for low propeller diameter geometry 3 has a better behaviour due to the great number of degrees of freedom.

## Conclusions

It is concluded that different aircraft configurations can be used in order to perform transport, surveillance and humanitarian aid mission.

The most efficient configuration is canard. However this kind of geometry has weaker longitudinal stability (high possibility to destabilize the airplane in case of moving the center of gravity backward and low possibility of moving it forward in comparison with three surface configuration) and will require autopilot if the centre of gravity changes during flight. To solve this problem three surface configuration can be used. This geometry presents higher efficiency than conventional configuration but similar behaviour. In addition, it also offers strong longitudinal stability and centre of gravity can move much more than in canard and conventional air-

craft without changes in eigenvalues. Moreover, this configuration can also be used in order to increase aerodynamic efficiency because of the additional degree of freedom. However, three surface configuration requires more complicated geometry and mechanism. For these reasons, it is less usual than conventional geometry.

On the other hand, conventional aircraft offers good stability and similar performance than other configurations. It is less efficient but is well known for this reason it is usually used in UAVs.

Finally, the selection of the geometry depends on the operation of the airplane. For high performance operation the better configuration is canard configuration. For variable center of gravity position, three surface configuration is the most stable. If the airplane has a defined operation without variation of the center of gravity and it is not flying in the limits of the flight domain, conventional geometry is recommended because of the geometry simplicity.

## References

- [1] R. FINK, *USAF STABILITY AND CONTROL DATCOM*, McDonnell Douglas Corporation.
- [2] J. GORDON LEISHMAN, *Principles of Helicopter Aerodynamics*, Second Edition. MARCELLO R. NAPOLITANO, *Aircraft Dynamics from Modeling to Simulation*, December 2012.
- [3] <http://upcventuri.com/castellano/nosotros>
- [4] <https://trenalosteam.wordpress.com/>
- [5] *XFLR5 Analysis of foils and wings operating at low Reynolds numbers*, October 2009.  
*Airplane flight dynamics and automatic flight controls*, 1979.

- [6] E. TORENBEEK and H. WITTENBERG, *Flight Physics. Essentials of Aeronautical Disciplines and Technology with Historical Notes.*
- [7] SNORRI GUDMUNDSSON, *General Aviation Aircraft Design: Applied Methods and Procedures.*
- [8] BLAIR B. GLOSS and LINWOOD W. MCKINNEY, *Canard-wing lift interference related to maneuvering aircraft at subsonic speeds.*

# Appendix

## Flight equations

$$m (\dot{V} + qV\alpha - rV\beta) = T + F_x - mg \sin\theta \quad (33)$$

$$m (\dot{V}\beta + V\dot{\beta} + rV - pV\alpha) = F_y + mg \cos\theta \sin\phi \quad (34)$$

$$m (\dot{V}\alpha + V\dot{\alpha} + pV\beta - qV) = F_z + mg \cos\theta \cos\phi \quad (35)$$

$$F_x = -\frac{1}{2}\rho V^2 S'' (c_D - \alpha c_L) \quad (36)$$

$$F_y = \frac{1}{2}\rho V^2 S'' c_Y \quad (37)$$

$$F_z = -\frac{1}{2}\rho V^2 S'' (\alpha c_D + c_L) \quad (38)$$

$$\dot{p} = \frac{I_{zz}}{A}L + \frac{I_{xz}}{A}N + \frac{I_{xz}(I_{xx} - I_{yy} + I_{zz})}{A}pq + \frac{I_{zz}(I_{yy} - I_{zz}) - I_{xz}^2}{A}rq \quad (39)$$

$$\dot{q} = \frac{1}{I_{yy}}M + \frac{I_{zz} - I_{xx}}{I_{yy}}pr + \frac{I_{xz}}{I_{yy}}(r^2 - p^2) \quad (40)$$

$$r' = \frac{I_{xx}}{A}N + \frac{I_{xz}}{A}L + \frac{I_{xz}(I_{yy} - I_{xx} - I_{zz})}{A}rq + \frac{I_{xx}(I_{xx} - I_{yy}) + I_{xz}^2}{A}pq \quad (41)$$

$$A = I_{xx}I_{zz} - I_{xz}^2 \quad (42)$$

$$L = \frac{1}{2}\rho S'' b'' V^2 c_L \quad (43)$$

$$M = \frac{1}{2}\rho S'' c'' V^2 c_M \quad (44)$$

$$N = \frac{1}{2}\rho S'' b'' V^2 c_N \quad (45)$$

$$p = \dot{\phi} - \dot{\psi} \sin\theta \quad (46)$$

$$q = \dot{\theta} \cos\phi + \dot{\psi} \cos\theta \sin\phi \quad (47)$$

$$r = \dot{\psi} \cos\theta \cos\phi - \dot{\theta} \sin\phi \quad (48)$$

$$\frac{\partial x}{\partial t} = u \cos\psi \cos\theta + v (\cos\psi \sin\theta \sin\phi - \cos\phi \sin\psi) + w (-\cos\psi \sin\phi + \cos\phi \sin\theta \sin\psi) \quad (49)$$

$$\frac{\partial y}{\partial t} = u \sin \psi \cos \theta + v (\sin \psi \sin \theta \sin \phi - \cos \phi \cos \psi) + w (-\cos \psi \sin \phi + \cos \phi \sin \theta \sin \psi) \quad (50)$$

$$\frac{\partial z}{\partial t} = -u \sin \theta + v \cos \theta \sin \phi + w \cos \theta \cos \phi \quad (51)$$

## Pathlines: wing configurations

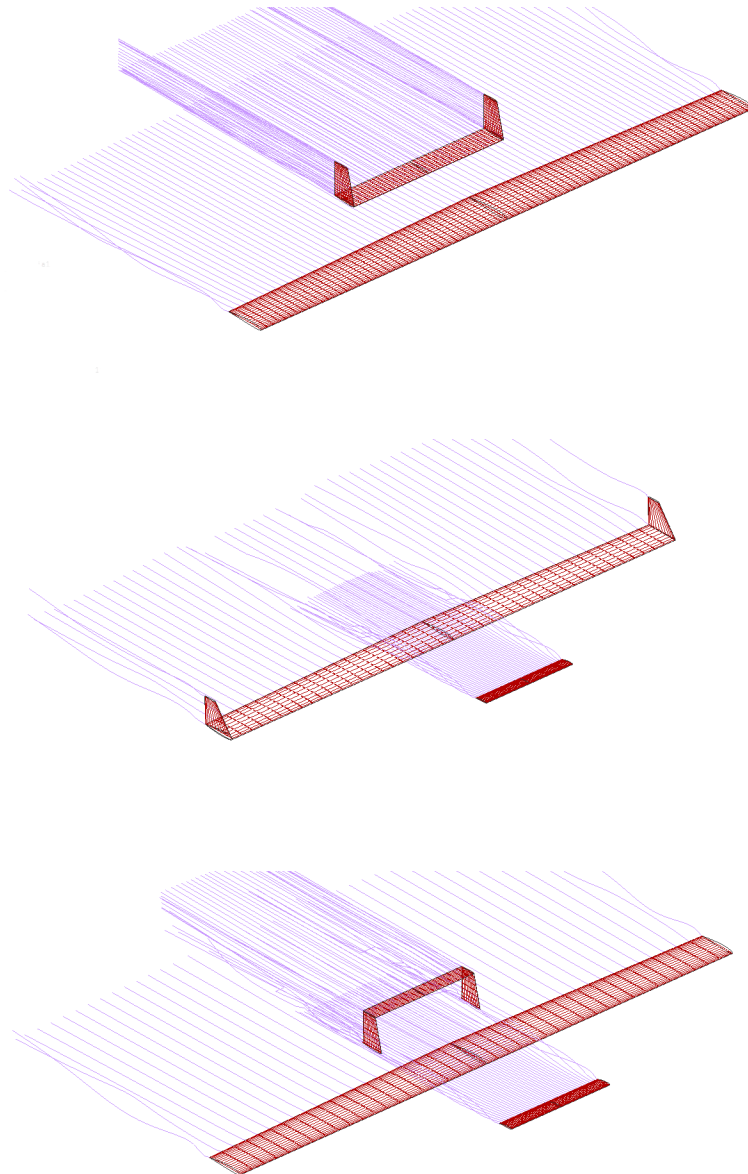


Figure 21: Pathlines (obtained with xflr5 [5]): geometry 1 (top), geometry 2 (middle), geometry 3 (bottom).

# Eigenvalues geometry 1

NOTE: Blank map means that the eigenvalue only presents real part.

## Longitudinal

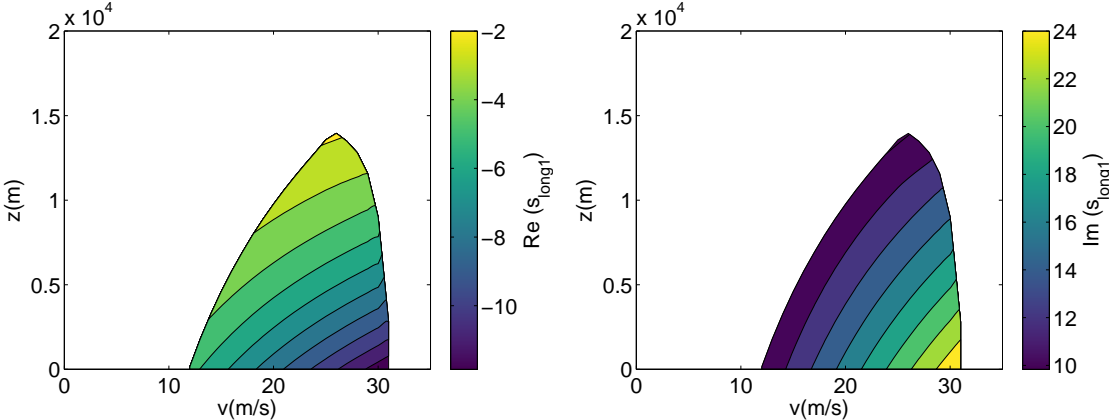


Figure 22: Real part (right) and imaginary part (left) of eigenvalue lateral-directional 1.

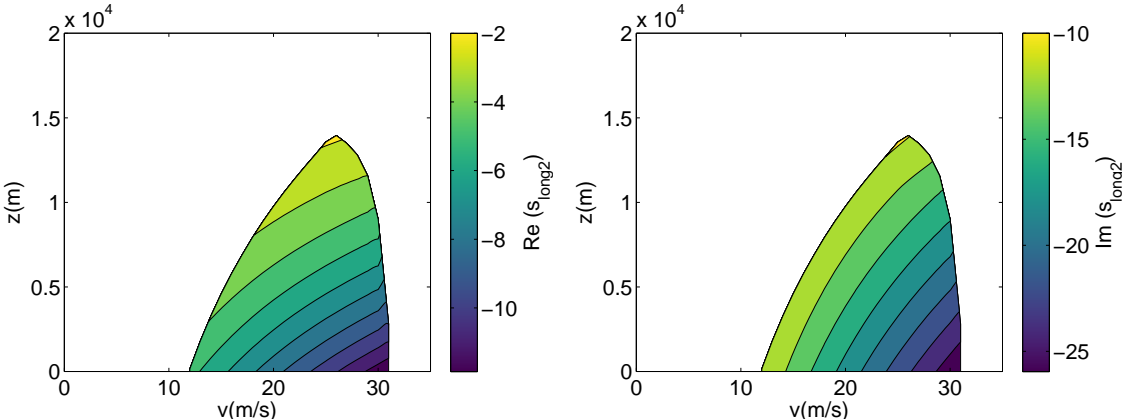


Figure 23: Real part (right) and imaginary part (left) of eigenvalue lateral-directional 2.

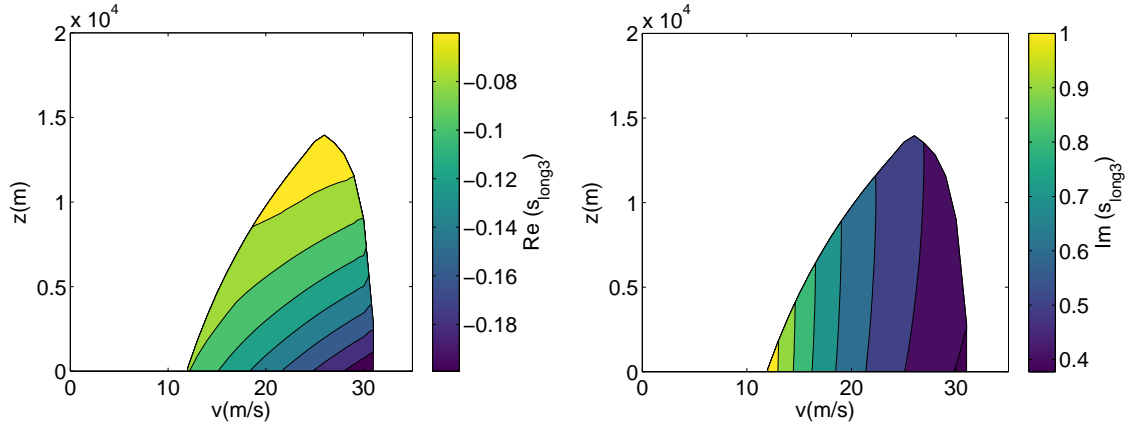


Figure 24: Real part (right) and imaginary part (left) of eigenvalue lateral-directional 3.

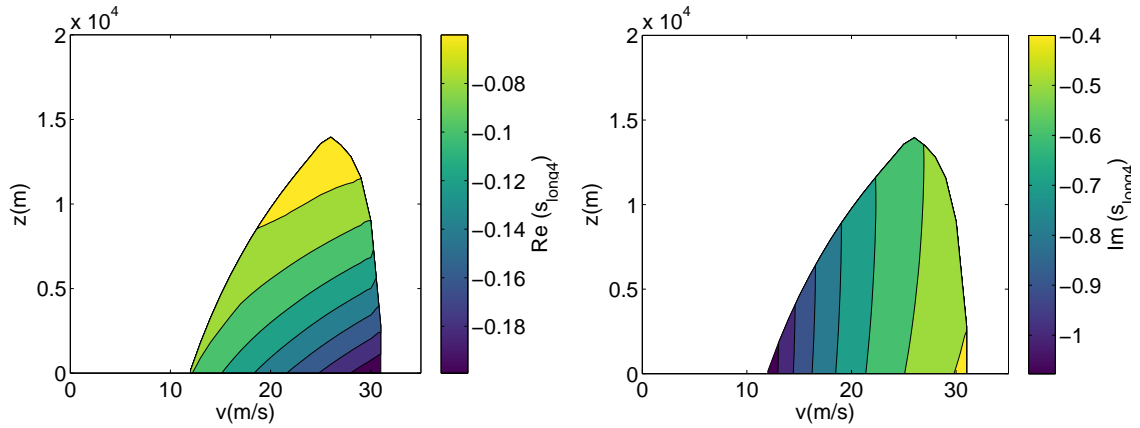


Figure 25: Real part (right) and imaginary part (left) of eigenvalue lateral-directional 4.

### Lateral-directional

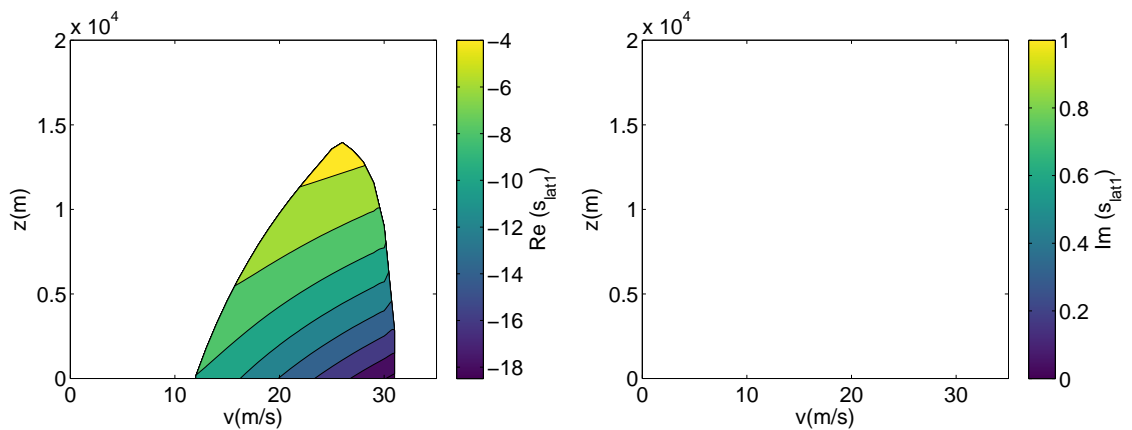


Figure 26: Real part (right) and imaginary part (left) of eigenvalue lateral-directional 1.

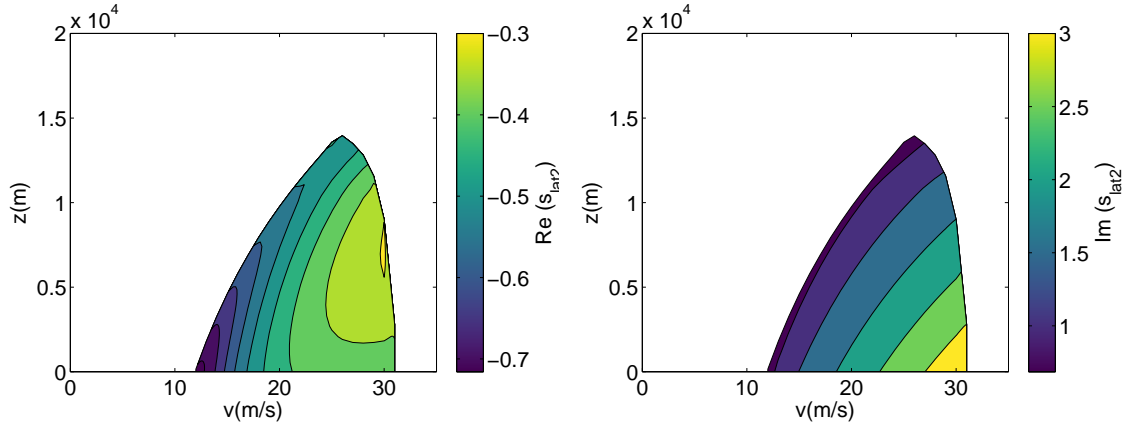


Figure 27: Real part (right) and imaginary part (left) of eigenvalue lateral-directional 2.

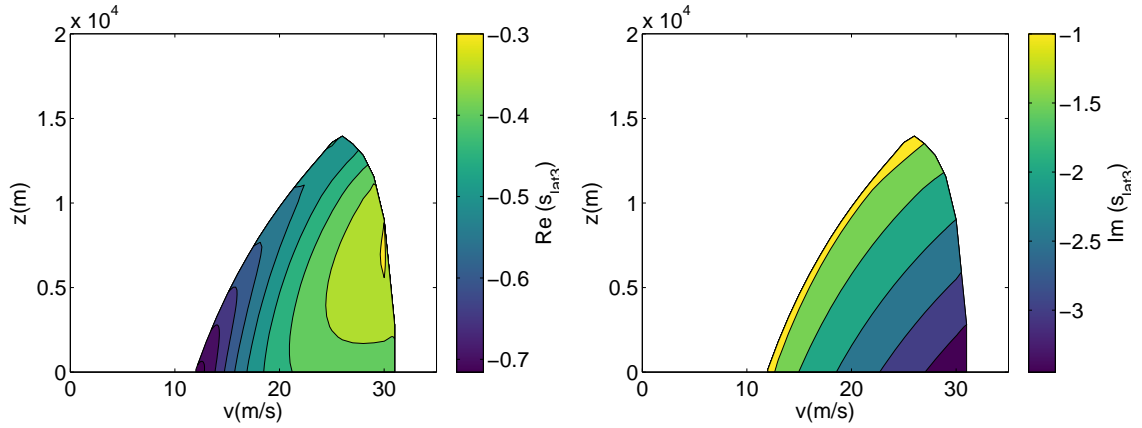


Figure 28: Real part (right) and imaginary part (left) of eigenvalue lateral-directional 3.

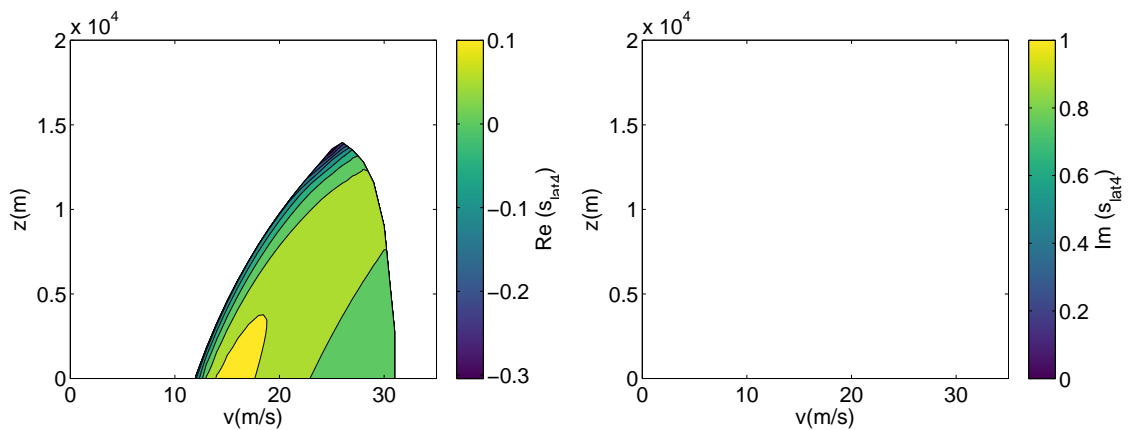


Figure 29: Real part (right) and imaginary part (left) of eigenvalue lateral-directional 4.

# Eigenvalues geometry 2

NOTE: Blank map means that the eigenvalue only presents real part.

## Longitudinal

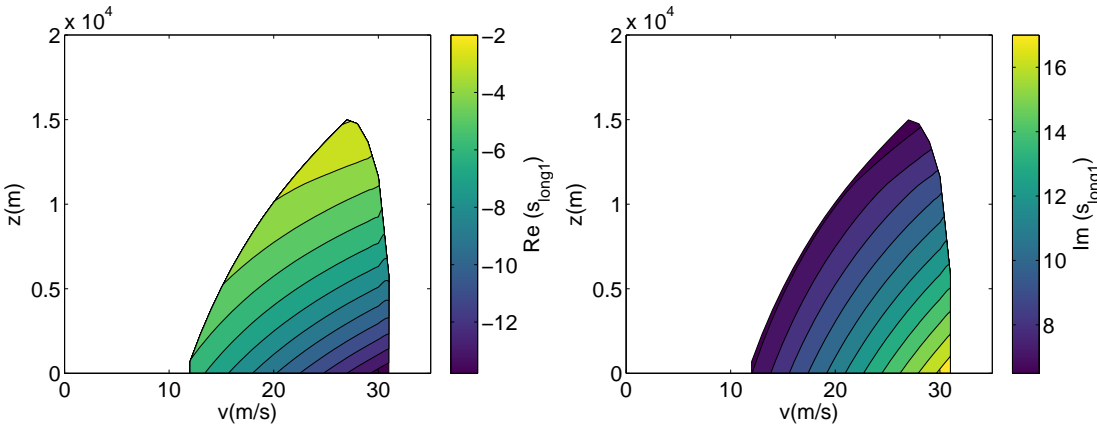


Figure 30: Real part (right) and imaginary part (left) of eigenvalue lateral-directional 1.

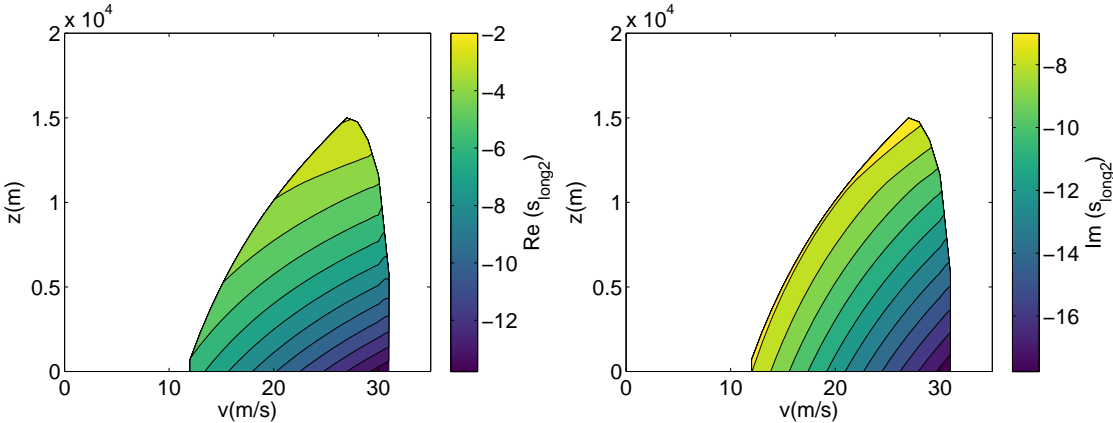


Figure 31: Real part (right) and imaginary part (left) of eigenvalue lateral-directional 2.

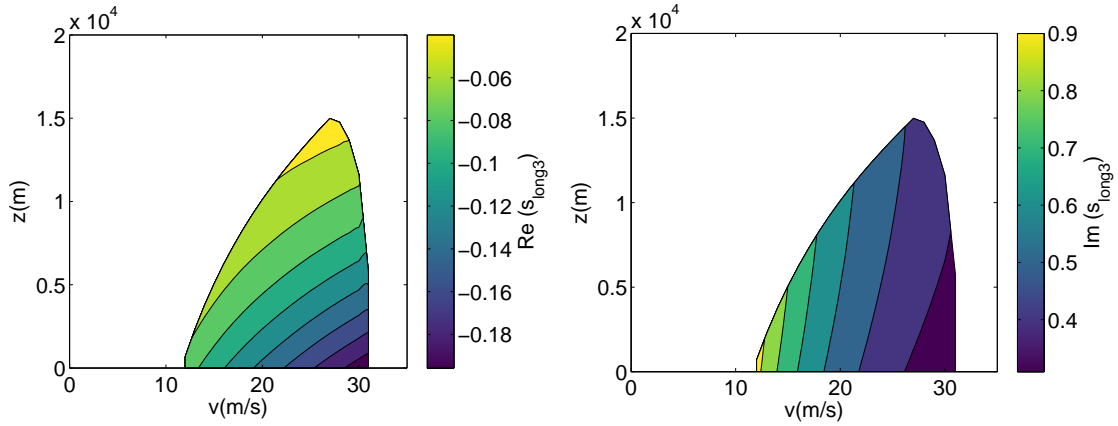


Figure 32: Real part (right) and imaginary part (left) of eigenvalue lateral-directional 3.

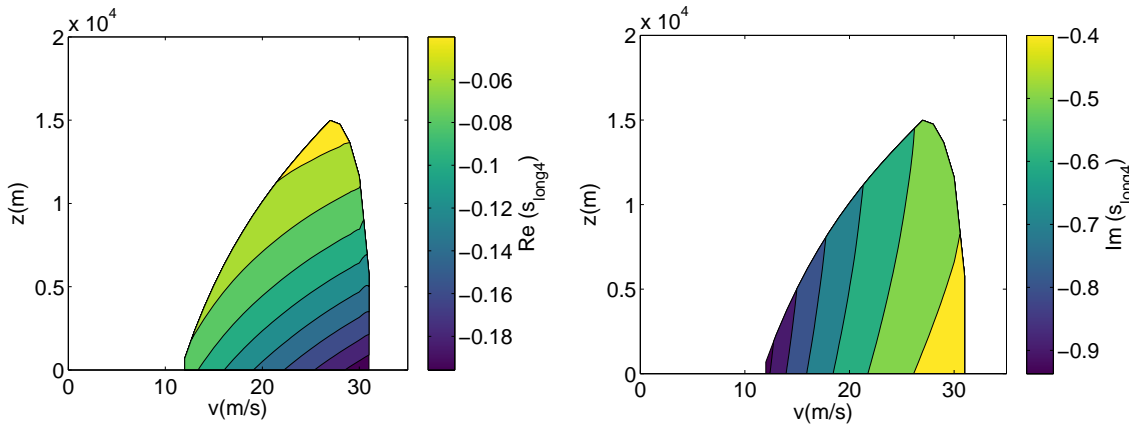


Figure 33: Real part (right) and imaginary part (left) of eigenvalue lateral-directional 4.

### Lateral-directional

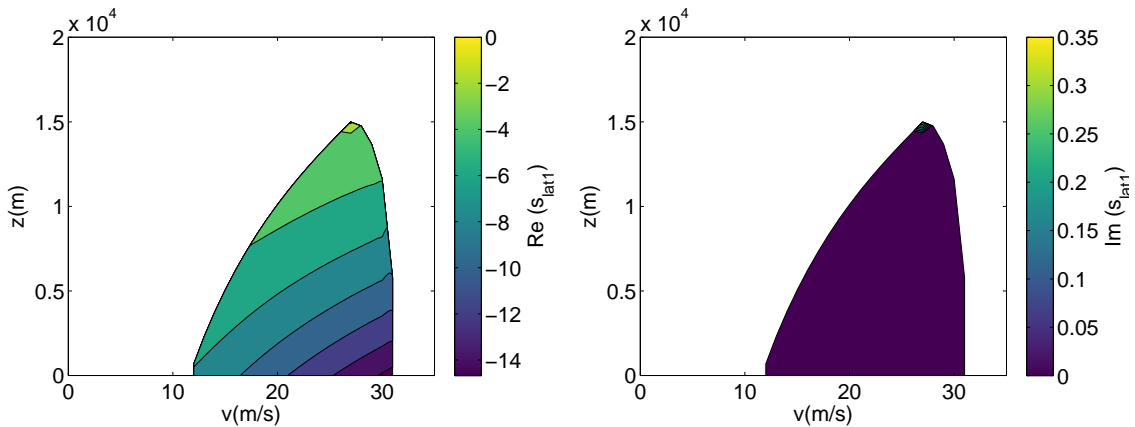


Figure 34: Real part (right) and imaginary part (left) of eigenvalue lateral-directional 1.

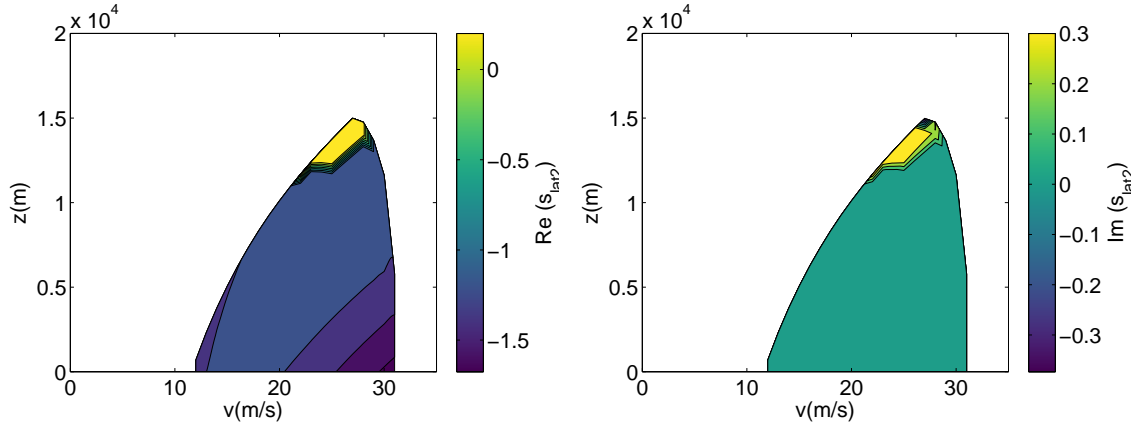


Figure 35: Real part (right) and imaginary part (left) of eigenvalue lateral-directional 2.

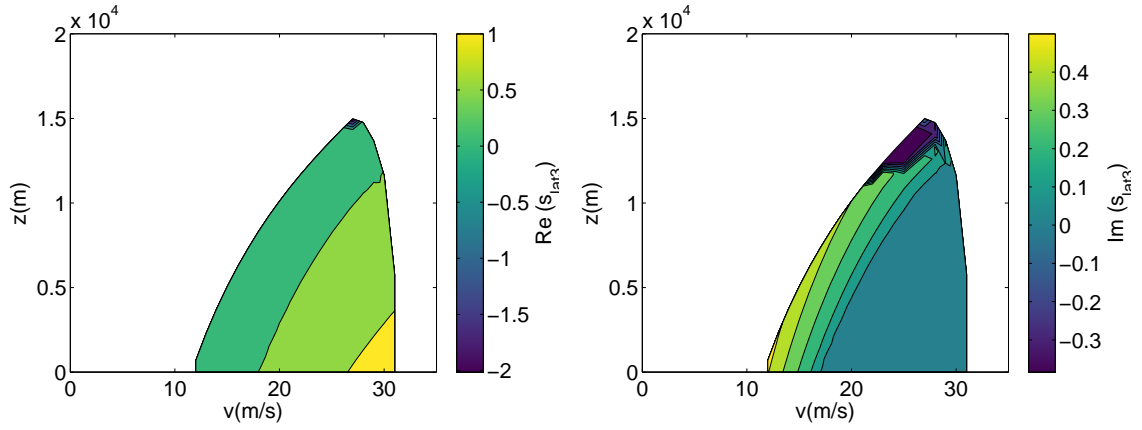


Figure 36: Real part (right) and imaginary part (left) of eigenvalue lateral-directional 3.

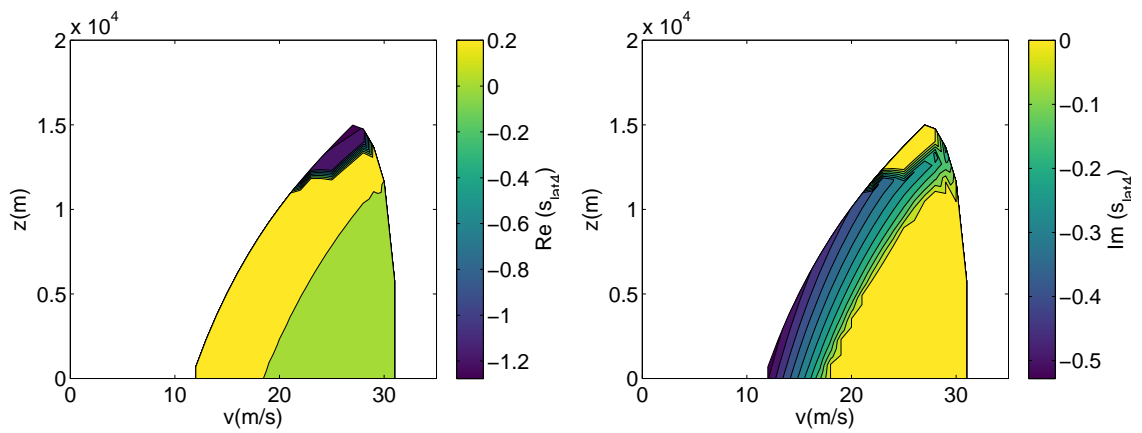


Figure 37: Real part (right) and imaginary part (left) of eigenvalue lateral-directional 4.

### Eigenvalues geometry 3

NOTE: Blank map means that the eigenvalue only presents real part.

#### Longitudinal

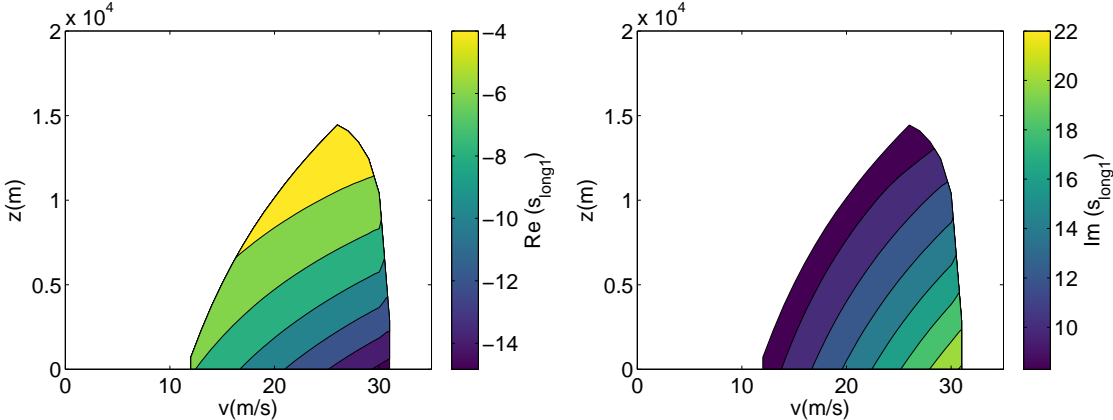


Figure 38: Real part (right) and imaginary part (left) of eigenvalue lateral-directional 1.

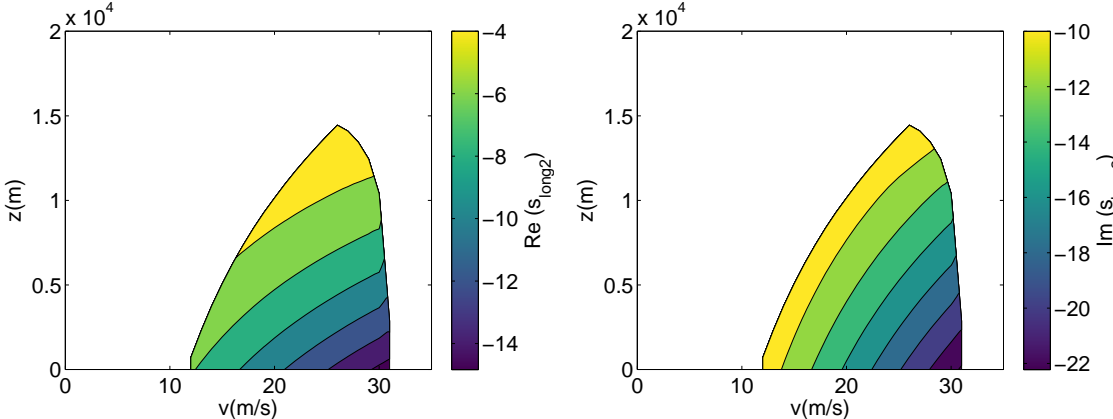


Figure 39: Real part (right) and imaginary part (left) of eigenvalue lateral-directional 2.

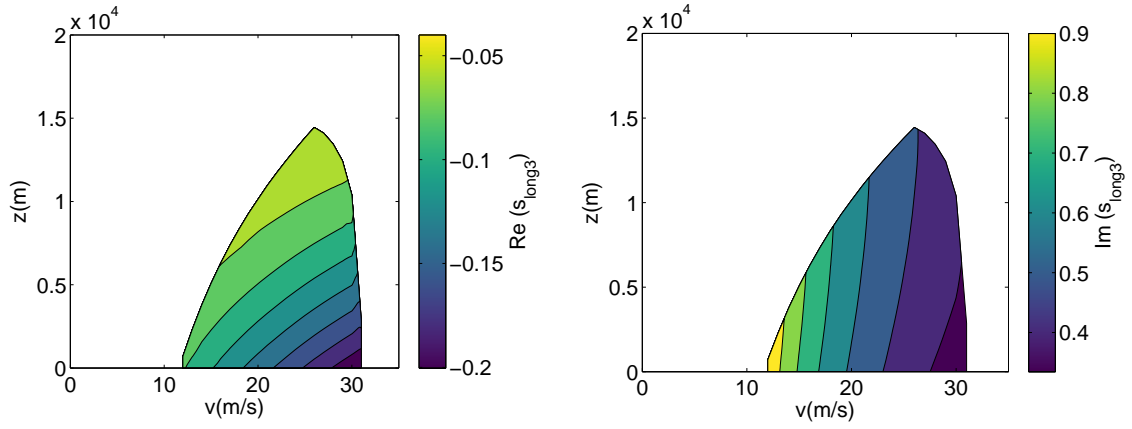


Figure 40: Real part (right) and imaginary part (left) of eigenvalue lateral-directional 3.

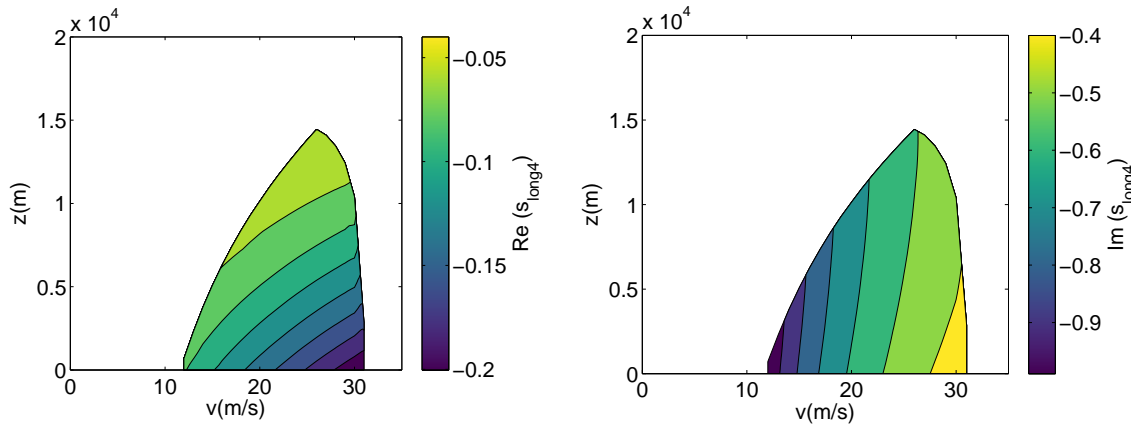


Figure 41: Real part (right) and imaginary part (left) of eigenvalue lateral-directional 4.

### Lateral-directional

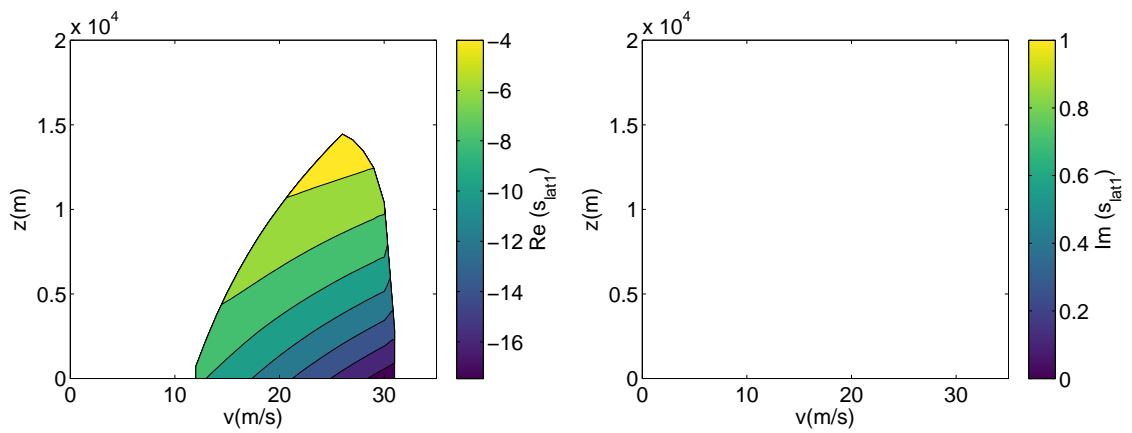


Figure 42: Real part (right) and imaginary part (left) of eigenvalue lateral-directional 1.

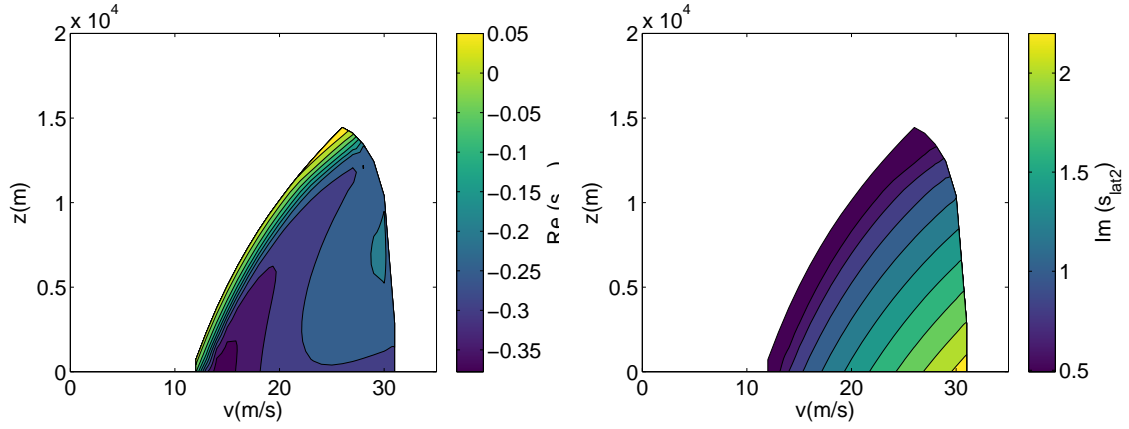


Figure 43: Real part (right) and imaginary part (left) of eigenvalue lateral-directional 2.

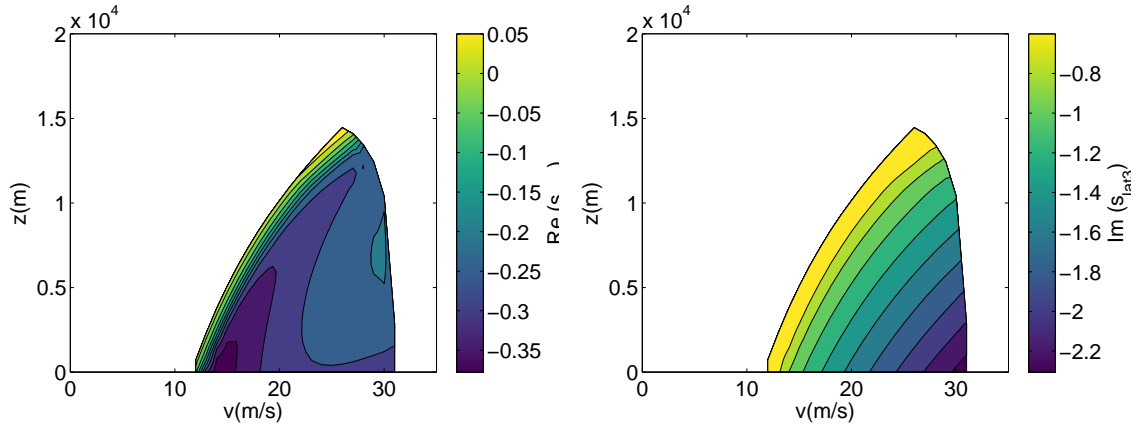


Figure 44: Real part (right) and imaginary part (left) of eigenvalue lateral-directional 3.

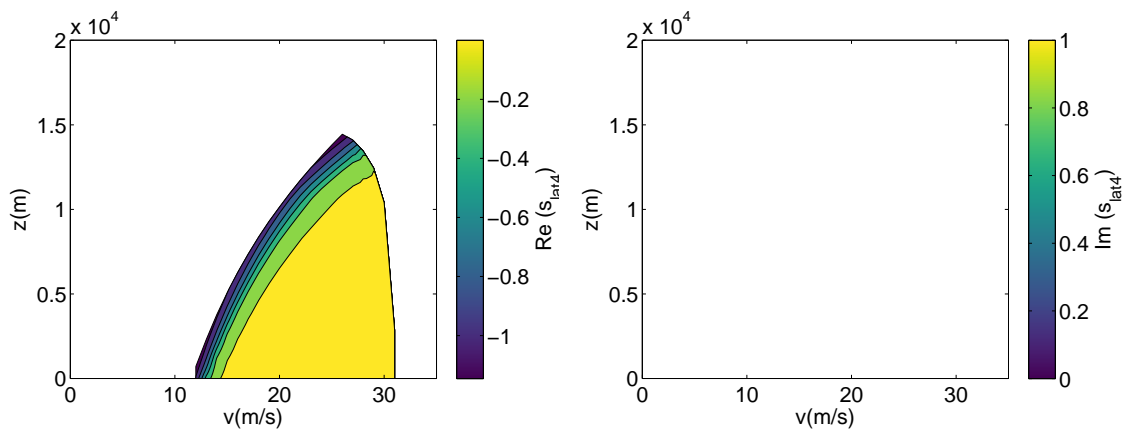


Figure 45: Real part (right) and imaginary part (left) of eigenvalue lateral-directional 4.

# Range and autonomy: Geometry 1

## Transport operation

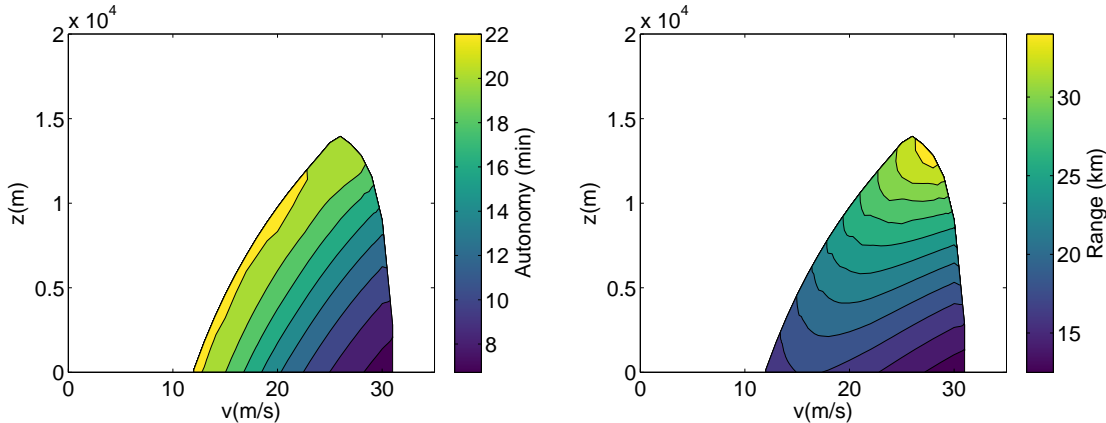


Figure 46: Autonomy (left) and range (right) of geometry 1.

## Surveillance operation

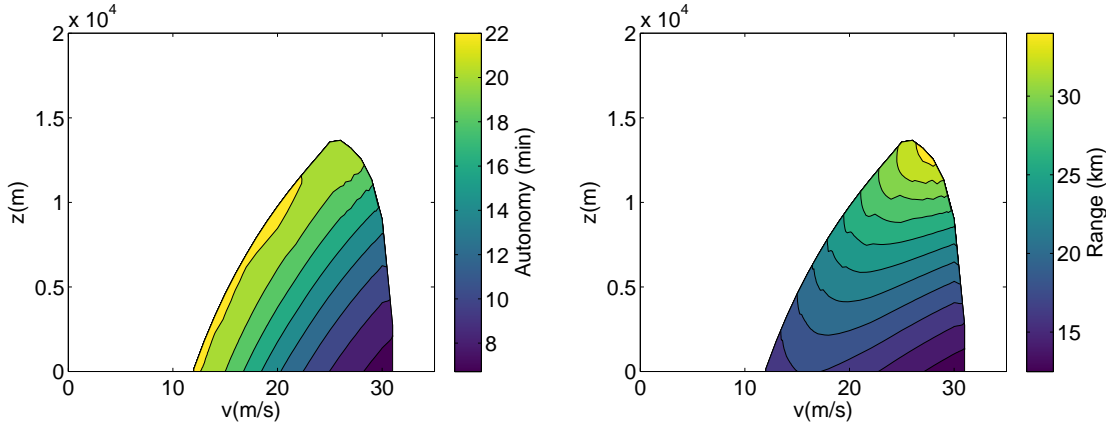


Figure 47: Autonomy (left) and range (right) of geometry 1.

humanitarian aid operation

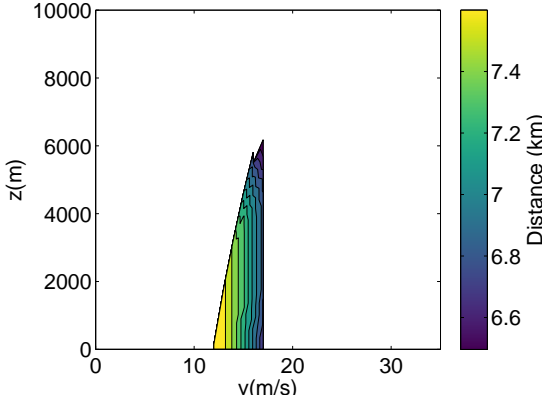


Figure 48: Maximum distance of human aid operation.

Range and autonomy: Geometry 2

Transport operation

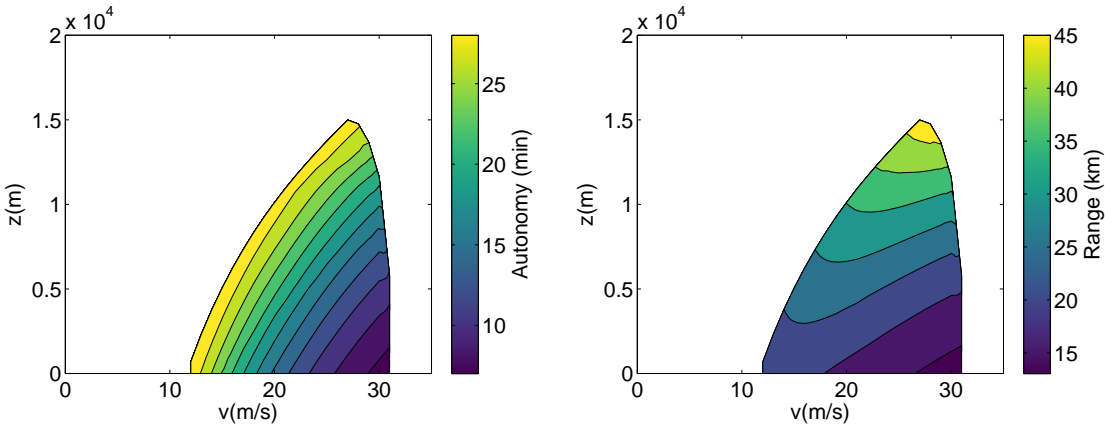


Figure 49: Autonomy (left) and range (right) of geometry 1.

### Surveillance operation

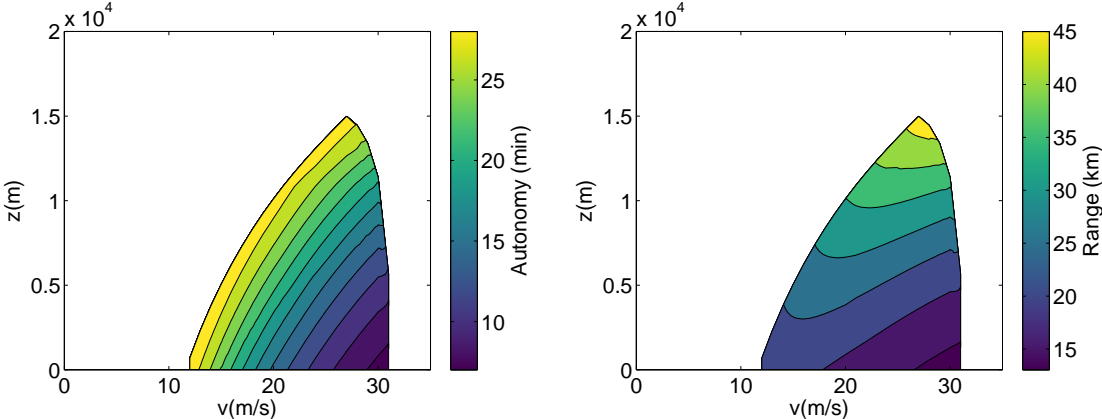


Figure 50: Autonomy (left) and range (right) of geometry 1.

### Humanitarian aid operation

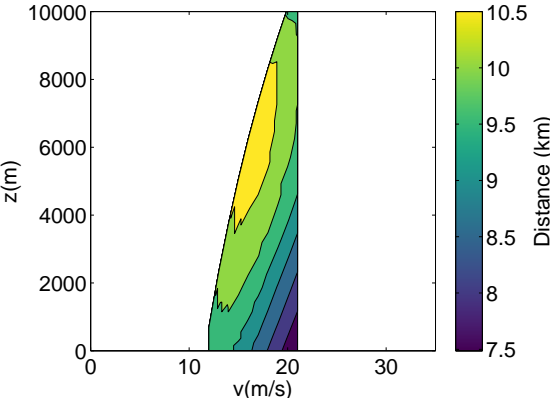


Figure 51: Maximum distance of human aid operation.

# Range and autonomy: Geometry 3

## Transport operation

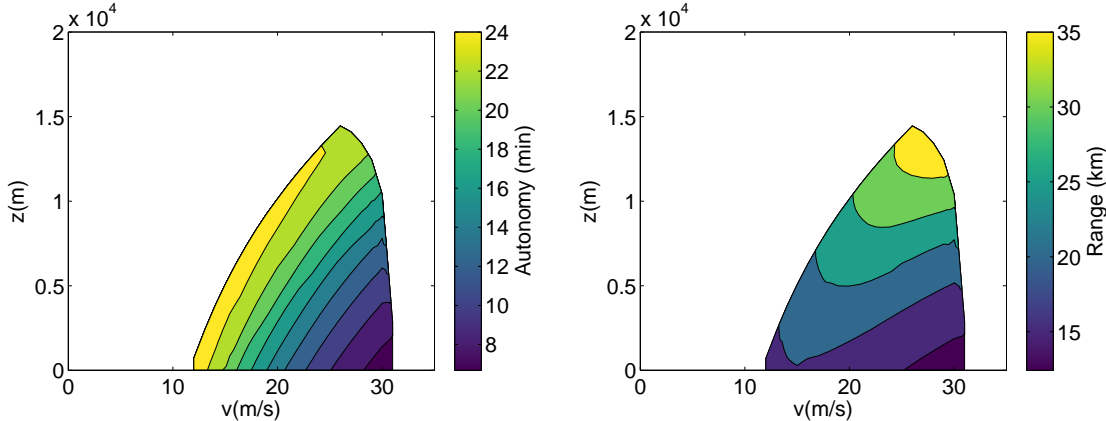


Figure 52: Autonomy (left) and range (right) of geometry 3.

## Surveillance operation

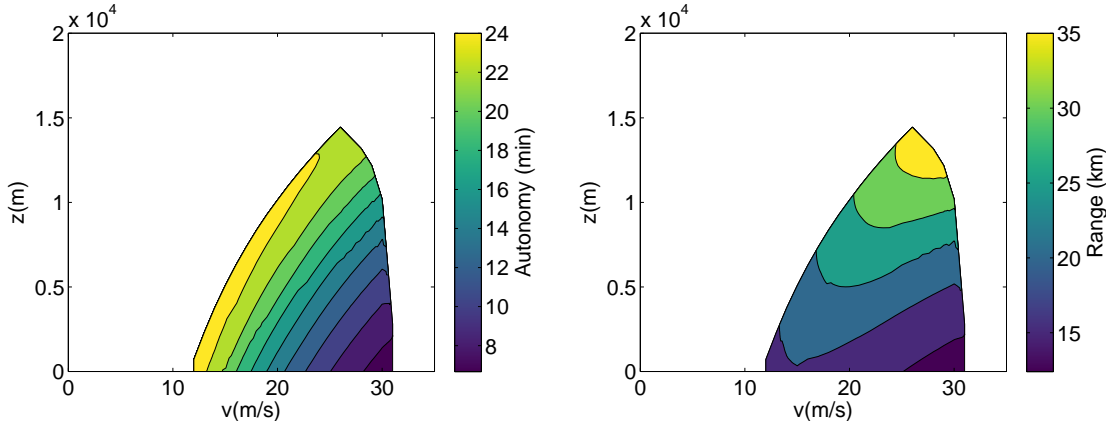


Figure 53: Autonomy (left) and range (right) of geometry 3.

humanitarian aid operation

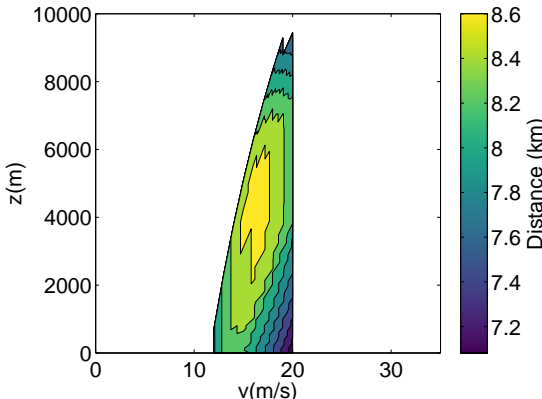


Figure 54: Maximum distance of human aid operation.